

# Thickness dependence of the morphology of ultrathin quench condensed gold films

K. L. Ekinici and J. M. Valles, Jr.

Department of Physics, Brown University, Providence, Rhode Island 02912

(Received 26 February 1998)

We have studied, using *in situ* scanning tunneling microscopy, the morphology of ultrathin quench condensed Au films in the thickness range in which they first become electrically continuous. With increasing thickness, the film evolves from a smooth and nearly featureless morphology, to a single layer of nanoclusters, to a loose pack of multiple layers of nanoclusters. This evolution depends only weakly on the substrate material and preparation. We compare our results to previously proposed models of quench condensed film structure. [S0163-1829(98)01536-7]

The electrons confined within the dimensions of an ultrathin film form the simplest, and perhaps most studied realization of a quasi-two-dimensional electron system. One method for producing ultrathin films is to evaporate metals onto substrates held at low temperatures,  $T_s < 0.1T_M$ , where  $T_M$  is the element's melting temperature. The advantages of quench condensed (QC) films have been exploited in a number of elegant and unique studies of fundamental issues in superconductivity,<sup>1-3,4</sup> localization,<sup>5-7</sup> and quantum phase transitions.<sup>8,9</sup> A distinct disadvantage of QC films is that they are metastable and, as a result, their microstructure, which can exert a profound influence on their electronic transport properties, has been difficult to characterize. For the interpretation of many experiments, it has been sufficient to assume that QC films exist in either a uniform<sup>4,6,7,9</sup> or islanded structure.<sup>8,10-13</sup>

Recently, the existence of islands in QC films has been questioned.<sup>14,15</sup> Nominal explanations of island formation that rely on thermally activated adatom diffusion fail for QC films because adatoms are believed to stick where they land.<sup>2,3,14-18</sup> In accord with this belief, many ultrathin QC single element metal films (e.g., Bi, Ga, Fe, Yb) form in metastable amorphous phases that are electrically continuous at mass depositions equivalent to a bulk thickness (dose equivalent thickness) as low as  $d = 1$  nm.<sup>19</sup> On the other hand, x-ray and electron microscopy studies on QC Au, Cu, Ag, Pb, and Cs films thicker than 10 nm show them to consist of microcrystallites.<sup>18-21</sup> Their critical thickness for the onset of conduction,  $d_G$ , depends on material and varies from 0.7 to more than 10 nm.<sup>19</sup> These observations have been interpreted as evidence for an islanded morphology in which macroscopic conduction occurs through interisland electron tunneling.<sup>4,8,10-13</sup> Alternatively, it has been proposed that all QC films initially begin in a continuous amorphous insulating phase, and, at the critical thickness for conduction, crystallites grow within the amorphous layer.<sup>14,15</sup>

We present results from a systematic, *in situ* scanning tunneling microscopy (STM) study of QC Au films on various substrates with thicknesses in the range at which conduction first begins. The topographs suggest that QC Au films form an amorphous phase that transforms into a crystalline phase with increasing thickness.<sup>14,15</sup> This transformation occurs below the critical thickness for conduction for Au on glass,  $d_{GAu}$  (Ref. 8) and it produces a single layer of nano-

clusters with heights that correspond closely to the thickness at which the transformation occurs. Thicker films consist of stacks of nanoclusters.

The low-temperature STM cryostat with *in situ* thermal evaporation sources used for these studies has been described in detail elsewhere.<sup>22</sup> Briefly, the chamber containing the STM and thermal evaporation sources was cooled to cryogenic temperatures by direct immersion in liquid helium or nitrogen. Prior to immersion, a turbo pump evacuated the system to  $< 2 \times 10^{-7}$  Torr. We estimate that the cryopumping action of the chamber walls reduced this pressure to  $< 10^{-8}$  Torr in liquid nitrogen and  $10^{-10}$  Torr in liquid helium. To make films, high-purity metals were thermally evaporated from resistively heated tungsten filaments at a rate of 0.1–1 Å/s as measured by a quartz crystal microbalance. A mechanical shutter was used to control the total deposition thickness and to outgas the source prior to exposing it to the substrate. A carbon resistance thermometer indicated that the substrate temperature increased less than 15 and 1 K during the depositions on 4 and 77 K substrates, respectively.

Images of Au films deposited on highly oriented pyrolytic graphite (HOPG), a substrate to which the adatoms physisorb and on amorphous Ge, a substrate to which the Au adatoms chemisorb are presented. HOPG is metallic, and, therefore, electrons can tunnel into it should the STM tip encounter a bare patch in the Au film, and its surfaces are simple to clean.<sup>23,24</sup> The most extensive cleaning processes were *in situ* cleaving of HOPG or heating air cleaved HOPG to 150 °C for 2 h in the UHV conditions created by immersing the cryostat in liquid helium. The STM results presented here were independent of the cleaning processes used. The amorphous Ge substrates were prepared by *in situ* quench condensation of 3–10 ML of Ge on glass or HOPG prior to the Au film deposition.<sup>25</sup> Topographs of films with  $1.2 < d < 6$  nm on HOPG and  $1 < d < 4$  nm on Ge were obtained to investigate the morphology of films in the thickness range at which conduction begins for Au on weak binding substrates (e.g.,  $d_G \approx 2.5$  nm for glass<sup>8</sup>) and on strong binding substrates [e.g.,  $d_G \approx 1$  nm for *a*-Ge (Ref. 6)], respectively.

The STM was operated in constant current mode at a bias voltage ranging from 7 to 500 mV and a tunneling current ranging from 0.5 to 10 nA. At these tunneling resistances there was no evidence that tip sample interactions influenced

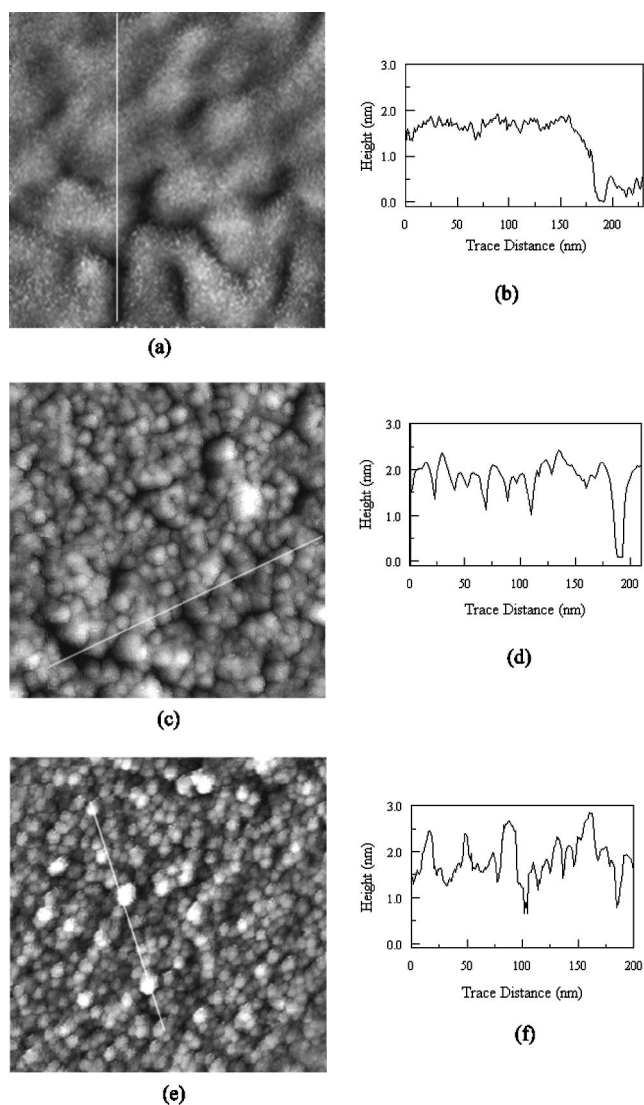


FIG. 1. *In situ* STM images of Au films with increasing thicknesses deposited on HOPG substrate at 4 K. The full scale height range from black to white is 2 nm for all images. The film thicknesses and scan areas are (a)  $d = 1.6 \pm 0.1$  nm and  $233 \times 233$  nm, (c)  $d = 1.8 \pm 0.1$  nm and  $210 \times 210$  nm and (e)  $d = 2.2 \pm 0.1$  nm and  $228 \times 228$  nm. The corresponding line scans are displayed in (b), (d), and (f). Note the exaggerated height scale.

the topographs or film structure. Tips were prepared using a variety of methods<sup>26</sup> as the imaging of thin films on flat substrates can be sensitive to STM tip geometry.<sup>27–29</sup> Each experiment was performed several times. The results that we present are independent of the particular method employed.

The morphology of ultrathin QC Au films on 4 K HOPG substrates depends strongly on thickness. As shown in Fig. 1(a), a  $d = 1.6 \pm 0.1$  nm film covers flat substrate areas uniformly and exhibits very small height variations in comparison to its thickness over distances of a few hundred nm. Breaks in the film expose the HOPG surface and the film height above the surface and the dose equivalent thickness agree within uncertainties [see Fig. 1(b)]. Large area images (not shown) suggest that these films are not structurally continuous on macroscopic length scales. In stark contrast, a slightly thicker film,  $d = 1.8 \pm 0.1$  nm, consists of islands.

The island tops are flat to 1 or 2 atomic layers over distances up to 10 nm. On some, height variations matching the atomic 111 steps in crystalline Au appear. A fraction of the gaps present between islands have atomically flat bottoms that we associate with the HOPG substrate [see Fig. 1(d)]. Relative to the bottoms of these gaps, the film thickness averaged over the area of the topograph is  $2.05 \pm 0.14$  nm, which is very close to, but larger than, the nominal deposited thickness. This difference implies that spaces between the clusters are not resolved completely. Line scans indicate that these films are in the microscopically rough surface regime,<sup>28</sup> i.e., the tip resolution is determined by an atomic-scale protrusion from the larger tip apex. An analysis of several line scans such as the one shown in Fig. 1(d) (Ref. 29) produces a tip apex radius  $r < 1$  nm and a cone angle  $\varphi \approx 30^\circ$ . This extremely sharp protrusion, however, is probably not long enough to clearly resolve all the gaps between the clusters.

As shown by Figs. 1(e) and 1(f), a slightly thicker film,  $d = 2.2 \pm 0.1$  nm, consists of similar flat-topped nanoclusters, but exhibits a less uniform height profile than the  $d = 1.8$  nm film. The nonuniformity can be traced to nanoclusters that rise consistently 1–2 nm above their neighbors. These nanoclusters appear to obscure similar ones below them. The average lateral dimension of 50 of the highest clusters is 12 nm with a standard deviation of 2.1 nm. Assuming that the cluster heights range from 1 to 2 nm, we find that these platelet-shaped nanoclusters have a diameter to height aspect ratio that exceeds 7. This aspect ratio and the fact that the clusters are raised well above the rest of the surface ensure that the tip geometry does not significantly influence these size measurements.

Variations in the substrate temperature over  $4 < T_s < 80$  K, film thickness up to 50 nm, and surface preparation methods did not strongly affect the nanocluster size. The thickness at which nanoclusters appeared was the same for 4- and 77-K depositions. Since crystalline structure in Au films with  $d > 15$  nm has been observed by other methods,<sup>1,18–21</sup> we conclude that the nanoclusters are crystalline. In addition, similar nanoclusters dominate the structure of films deposited on glass ( $d = 11$  nm), crystalline Au ( $d = 1.7$  nm), and *in situ* deposited amorphous Ge ( $d = 3.2, 4.0$  nm).

The morphology of Au films deposited on amorphous Ge depends on thickness in a qualitatively very similar manner to Au films on HOPG. The  $d = 2.0$  nm film is smooth and does not contain nanoclusters, whereas a  $d = 3.2$  nm film does contain nanoclusters [Figs. 2(a) and 2(b)]. The undulations in the thinner film on Ge are not as strong as the “breaks” in the thinner film on HOPG, but their profiles are comparable.

Warming (annealing) Au films on HOPG with thicknesses  $2.1 < d < 10.0$  nm to room temperature produces cracks in the films, but does not change the cluster size [see Fig. 3(a)]. The cracks are randomly oriented and come in a large range of sizes and shapes, and the film surface at areas away from the cracks remains quite flat. The crack area range is 1–20% of a film’s surface, which is too large to be accounted for by simple differential thermal contraction.<sup>30</sup> Instead, these observations suggest that voids exist between the clusters of an as-deposited film and thermal annealing drives the clusters to pack more densely. Close inspection of the crack bottoms

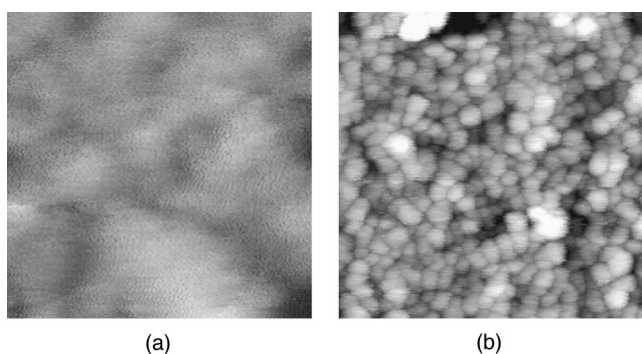


FIG. 2. *In situ* STM images of Au films with different thicknesses deposited at 77 K on amorphous Ge layers. The amorphous Ge was quench condensed *in situ* just prior to the Au deposition. The film thicknesses on glass substrate are (a)  $d_{\text{Au}} = 2.0 \pm 0.1$  nm,  $d_{\text{Ge}} = 3.2 \pm 0.2$  nm and (b)  $d_{\text{Au}} = 3.1 \pm 0.1$  nm,  $d_{\text{Ge}} = 1.2 \pm 0.1$  nm. Both scan areas are  $185 \times 185$  nm.

directly reveals the presence of an underlayer of grains with dimensions similar to those on the upper surface of the film [Figs. 3(a) and 3(b)].<sup>31</sup>

In support of the above picture, x-ray and electron microscopy studies indicate that films with  $d > 50$  nm of a wide range of metals, including Au, deposited on cold substrates form as a loose pack of crystalline nanoclusters. Moreover, these nanocrystals orient with a single crystalline axis perpendicular to the substrate plane.<sup>17,18</sup> In films of fcc metals the 111 axes of crystals closest to the substrate orient to minimize the substrate film interfacial, interaction energies.<sup>21,32</sup> Consequently, we propose that the nanoclusters in ultrathin QC Au films are crystalline (see earlier discussion) with their 111 axes perpendicular to the substrate.

The lack of nanoclusters and relatively smooth appearance of the thinnest Au films coincides with the unstructured, amorphous morphology expected for films deposited under conditions in which atoms stick where they land.<sup>14,15</sup> In the case of the amorphous Ge substrate, we expect that the covalent bonding between the Au and Ge stabilizes the first few Au layers in an amorphous phase. This expectation is partially based on the observations that quench condensed Ge and Ge mixed with noble metals is amorphous.<sup>33</sup> On length scales shorter than 50 nm, both films show only atomic-scale height variations. Neither film exhibits the

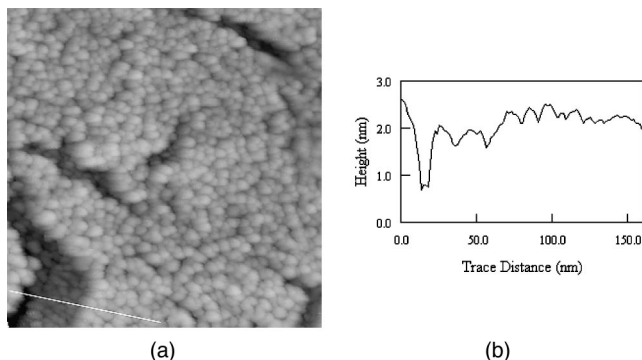


FIG. 3. (a) STM image of a  $d = 2.2$  nm Au film on HOPG deposited at 4 K, after being annealed to 300 K. The scan area is  $325 \times 325$  nm and the height range is 2.5 nm. (b) Line scan through the crack showing two layers of grains.

nanoclustered morphology characteristic of thicker films. The similar morphologies of thin Au/Ge and Au/HOPG films suggest that amorphous Au films form even on weak binding substrates and that the evolution of the morphology is independent of substrate. The former observation is noteworthy as all previous x-ray and electron microscopy measurements, which were limited to thicker films, suggested that only crystalline Au films formed.<sup>18,19</sup>

Similar thickness-dependent amorphous to polycrystalline transitions have been observed in QC Bi and Ga films<sup>19</sup> as well as in Sb and  $\text{InO}_2$  films deposited on higher-temperature substrates.<sup>34,35</sup> By contrast, however, the critical thicknesses for their transformations exceed 10 nm and in the case of Bi and Ga films at  $T_s = 4$  K,  $d_c \geq 100$  nm,<sup>19</sup> making it possible to observe them with electron microscopy and x-ray scattering. Qualitative descriptions of those transitions offer an explanation for the differences in  $d_c$ .<sup>16,19</sup> In very thin films, the lack of adatom mobility and strong interaction with the substrate forces the atoms into a disordered state. As a film becomes thicker, the influence of the substrate potential on the interatomic positions and spacings wanes, and the formation of nuclei with bulk atomic spacings becomes energetically favorable. At this point, neighboring atoms can become part of a nucleus through small (less than a lattice spacing) movements. The heat released in crystallization as neighboring atoms join a nucleus is thought to fuel the crystalline growth. The greater stability of the amorphous phases of QC Bi and Ga films can be understood to reflect the fact that their atomic bonds are more directional than those in a fcc metal like Au.<sup>16,19</sup> Consequently, the height of potential barriers hindering the motion of atoms to positions expected in an equilibrium crystal structure are larger in Bi than in Au.<sup>16,19</sup>

The growth of similar grains on top of the first layer of grains [see Figs. 1(b) and 1(c)] implies that a transformation process similar to that described above occurs continuously during quench condensation. We propose that the uppermost surface of a growing film consists of grains that have stable sizes and shapes and untransformed amorphous patches. The roughness of the substrate formed by the existing grains restricts the lateral dimensions of these patches to about the size of the grains. Once their local thickness exceeds a critical value, a new grain nucleus forms. Important support for this view comes from the observations of grains that are higher than their neighbors [see Fig. 1(c)] by an amount that closely corresponds to the critical thickness for the formation of a polycrystalline film. The most direct evidence for this model would be images of the amorphous patches. If grains and patches are the same size, however, it would be difficult to resolve their differences in a topograph. This overall picture of the grain formation agrees with an earlier model used to account for the formation of grains in much thicker films of a wide range of metals deposited on cold substrates.<sup>18</sup>

The exact mechanisms governing grain formation in QC films remain unsettled. The narrow size distribution of the nanoclusters, their large aspect ratio, and their stability against thermal annealing over a factor of more than 20 in temperature may be important clues about the process.

Finally, we compare the film morphologies with the structures conjectured for the analysis of past electronic transport, tunneling, and photoemission experiments.<sup>4,8,10–13,36</sup> Those

conjectures, which were based on macroscopic transport<sup>4,6-13</sup> and tunneling measurements,<sup>37</sup> grouped the structures into two extreme categories, homogeneous or smooth and islanded or granular. Metal films thinner than about 1 nm deposited on amorphous semiconductor layers are conductive and have been assumed to be homogeneous.<sup>4,6,7,9</sup> The Au on Ge STM results [Fig. 2(b)] support this picture. Metal films deposited directly on weak binding substrates (e.g., glass) have been assumed to form a two-dimensional disordered array of islands at the thickness at which they first conduct.<sup>8,10-13</sup> The appearance of a nearly complete layer of nanoclusters with gaps between them in Au films with  $d < d_G$  for Au films on glass tends to support this assumption.

If this is correct, then it implies that the amorphous precursor layer is not macroscopically conductive. Whether this layer is a microscopically insulating form of Au, as has been proposed to exist for other metals, or has structural discontinuities that prevent conduction, remains as an open question.<sup>14,15</sup> Its resolution requires direct measurements of the transport and electronic properties of the unstructured phase.

We have benefited from discussions with C. Elbaum, X. S. Ling, M. Strongin, A. Truscott, G. Bergmann, and, especially, J. Kondev. This study was supported by the NSF through Grant Nos. DMR-9296192 and DMR-9502920, and partially by the ONR through Grant No. N00014-95-0747.

- <sup>1</sup>W. Buckel and R. Hilsch, Z. Phys. **138**, 109 (1954).
- <sup>2</sup>W. Buckel, Z. Phys. **138**, 136 (1954).
- <sup>3</sup>H. Bulow and W. Buckel, Z. Phys. **145**, 141 (1956).
- <sup>4</sup>M. Strongin, R. S. Thompson, and O. F. Kammerer *et al.*, Phys. Rev. B **2**, 4920 (1971).
- <sup>5</sup>G. Bergmann, Phys. Rep. **107**, 1 (1984).
- <sup>6</sup>S.-Y. Hsu and J. M. Valles, Jr., Phys. Rev. Lett. **74**, 2331 (1995).
- <sup>7</sup>Y. Liu *et al.*, Europhys. Lett. **19**, 409 (1992).
- <sup>8</sup>R. C. Dynes, J. P. Garno, and J. M. Rowell, Phys. Rev. Lett. **40**, 479 (1978).
- <sup>9</sup>D. B. Haviland, Y. Liu, and A. M. Goldman, Phys. Rev. Lett. **62**, 2180 (1989).
- <sup>10</sup>A. E. White, R. C. Dynes, and J. P. Garno, Phys. Rev. B **33**, 3549 (1986).
- <sup>11</sup>H. M. Jaeger, D. B. Haviland, A. M. Goldman, and B. G. Orr, Phys. Rev. B **34**, 4920 (1986).
- <sup>12</sup>R. P. Barber, Jr. and R. Glover III, Phys. Rev. B **42**, 6754 (1990).
- <sup>13</sup>R. S. Markiewicz, C. A. Shiffman, and W. Ho, J. Low Temp. Phys. **71**, 175 (1988).
- <sup>14</sup>A. V. Danilov, S. E. Kubatkin, I. L. Landau, I. A. Parshin, and L. Rinderer, Phys. Rev. B **51**, 5514 (1995).
- <sup>15</sup>A. V. Danilov, S. E. Kubatkin, I. L. Landau, and L. Rinderer, J. Low Temp. Phys. **103**, 1 (1996).
- <sup>16</sup>S. Fujime, Jpn. J. Appl. Phys. **6**, 305 (1967).
- <sup>17</sup>M. Ohring, *The Materials Science of Thin Films* (Academic, San Diego, 1991).
- <sup>18</sup>C. R. M. Governor, H. T. G. Hentzell, and D. A. Smith, Acta Metall. **32**, 773 (1984).
- <sup>19</sup>Y. F. Komnik, Sov. J. Low Temp. Phys. **8**, 1 (1982).
- <sup>20</sup>N. Yoshida, O. Oshima, and F. E. Fujita, J. Phys. F **2**, 237 (1972).
- <sup>21</sup>R. W. Vook and F. Witt, J. Vac. Sci. Technol. **2**, 49 (1965).
- <sup>22</sup>K. L. Ekinci and J. M. Valles Jr., Rev. Sci. Instrum. **68**, 4152 (1997).
- <sup>23</sup>T. P. Darby and C. M. Wayman, J. Cryst. Growth **28** (1975).
- <sup>24</sup>R. Nishitani, A. Kasuya, S. Kubota, and Y. Nishina, J. Vac. Sci. Technol. B **9**, 806 (1991).
- <sup>25</sup>B. Stritzker and H. Wuhl, Z. Phys. **243**, 361 (1971).
- <sup>26</sup>Experiments using mechanically cut, etched, and commercially acquired tips (Materials Analytical Services) with apex radius  $r \approx 50$  nm and cone angle  $\varphi \approx 7.5^\circ$ , have produced similar topographs.
- <sup>27</sup>J. K. Gimzewski, A. Humbert, J. G. Bednorz, and B. Reihl, Phys. Rev. Lett. **55**, 951 (1985).
- <sup>28</sup>G. Reiss, J. Vancea, H. Wittmann, J. Zweck, and H. Hoffmann, J. Appl. Phys. **67**, 1156 (1990).
- <sup>29</sup>G. Reiss, F. Schneider, F. Vancea, and H. Hoffmann, Appl. Phys. Lett. **57**, 867 (1990).
- <sup>30</sup>The thermal expansion coefficients at room temperature for HOPG and Au are  $20 \times 10^{-6} \text{ }^\circ\text{C}^{-1}$  and  $14.2 \times 10^{-6} \text{ }^\circ\text{C}^{-1}$ , respectively. To produce a crack area of 1% of a films surface would require a decrease in temperature of approximately 1600 K as estimated using these coefficients.
- <sup>31</sup>Line scans similar to Fig. 3(b) show that the tip is sharp enough to resolve the grains in the cracks. The tip that produced this image had an apex radius  $r < 1$  nm and a cone angle  $\varphi \approx 40^\circ$ . In addition, smaller area scans were inspected to determine if images of the grains in the cracks were replicas of the nearby upper layers and therefore, artifacts. No evidence of this was noticed.
- <sup>32</sup>C. V. Thompson, in *Polycrystalline Thin Films: Structure, Texture, Properties and Applications*, edited by K. Barmak, M. A. Parker, J. A. Floro, R. Sinclair, and D. A. Smith, MRS Symposia Proceedings No. 343 (Materials Research Society, Pittsburgh, 1994), p. 13.
- <sup>33</sup>E. Haug, N. Hedgecock, and W. Buckel, Z. Phys. B **22**, 237 (1975).
- <sup>34</sup>K. Maki, Jap. J. Appl. Phys. **19**, 2069 (1980).
- <sup>35</sup>S. Muranaka, Y. Bando, and T. Takada, Thin Solid Films **151**, 355 (1987).
- <sup>36</sup>D. J. Huang, G. Reisfeld, and M. Strongin, Phys. Rev. B **55**, R1977 (1997).
- <sup>37</sup>S.-Y. Hsu and J. M. Valles Jr., Phys. Rev. B **49**, 6416 (1994).